Nano Energy 116 (2023) 108804

Contents lists available at ScienceDirect

Nano Energy

journal homepage: www.elsevier.com/locate/nanoen

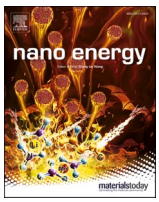

Molecular layer deposition to grow a luminescent metalorganic monolayer on inorganic substrate: Breaking monopoly of solution routes to self-assembled monolayer

Anna L. Pellegrino [a], Cristina Tudisco [a], Francesca Lo Presti [a], Emil Milan [b], Adolfo Speghini [b], Guglielmo G. Condorelli [a], Graziella Malandrino [a,*]

[a] Dipartimento Scienze Chimiche, Università degli Studi di Catania, and INSTM UdR Catania, Viale Andrea Doria 6, 95125 Catania, Italy
[b] Nanomaterials Research Group, Department of Biotechnology, University of Verona and INSTM RU Verona, Strada Le Grazie 15, I-37134 Verona, Italy

ARTICLE INFO

Keywords:
Monolayers
Europium complexes
Downshifting
Nickel oxide layer
Hybrid system
MLD

ABSTRACT

A gas-phase route such as molecular layer deposition has been applied for the first time to create a monolayer of metalorganic Eu(III) molecules on NiO oxide layer. The surface of the as-deposited NiO layer is activated using H_2O/O_2 vapors, and then functionalized by anchoring molecules of the Eu complex working at different temperatures to favor the chemisorption process. The effects of the activation process and of the MLD temperature on the chemisorption of the Eu complex were evaluated through in-depth X-ray photoelectron and luminescence spectroscopy studies. These analyses allowed to define the stoichiometry of the Eu moiety chemisorbed on the surface and the optimization of an impressive strategy to the synthesis of hybrid metalorganic/inorganic systems. The hybrid system's luminescence properties have proved the monolayer's energy conversion phenomena and produced further information about the local environment around the Eu(III) anchored as a complex on the NiO surface.

1. Introduction

In the last decades, the organic-inorganic hybrid systems, made of inorganic surfaces functionalized through covalent attachment of organic molecules, have attracted great attention because of their potential applications in several fields of material science [1–3], such as sensors [4,5], dye sensitized solar cells (DSSCs) or perovskite solar cells [6], optoelectronic devices [7,8], and heterogeneous catalysis [9,10]. In these systems, transition metal oxide thin films are the most promising inorganic materials [11,12] due to their wide spectrum of magnetic, electrical, and optical properties [13]. The anchoring of organic luminescent complexes on inorganic surfaces [14–16] leads to a plethora of new multifunctional materials with a wide range of modular properties, and therefore a comprehensive range of applications [17].

Up to date, most of the synthetic approach to prepare hybrid systems takes advantage of solution routes such as sol-gel procedure [18,19], Langmuir-Blodgett techniques [20,21], self-assembly solution route [22]. In conventional solution approaches, given the nature of the inorganic film active sites, the most common functional organic moieties, chosen for the hybrid approach, are molecules having silane [23,24], thiol [25] and carboxylic functionalities [26] as anchoring groups. As an alternative route also organophosphorous compounds have been tested as linkers for the functionalization of metal oxide surfaces [27]. Thus, these procedures may imply a double step process to anchor firstly the linker and then the functional molecules.

Nevertheless, scaling up of processes based on solution routes is not straightforward, and for a huge variety of applications, the possibility of a fast, highly efficient and reproducible assembly of molecules onto nanostructured substrates is of paramount importance.

Molecular layer deposition (MLD) is a solvent-free method, strictly related to atomic layer deposition [28], which takes advantage of the chemisorption self-limiting process to link organic monolayers on various substrates [29]. By combining the two techniques ALD and MLD, a significant step ahead has been done in the synthesis of new types of inorganic–organic hybrid materials [30], coordination-polymer- or metal–organic-framework-like structures [31]. In addition, MLD is an easily scalable process with the advantage of excellent conformal covering.

* Corresponding author.
E-mail address: graziella.malandrino@unict.it (G. Malandrino).

https://doi.org/10.1016/j.nanoen.2023.108804
Received 10 April 2023; Received in revised form 2 August 2023; Accepted 17 August 2023
Available online 19 August 2023

Given the nature of the MLD process, we have investigated the possibility to apply this synthetic route to the preparation of metalorganic/inorganic hybrid systems. As a case study we have focused our attention on a hybrid system consisting of a transition metal oxide as inorganic material and a luminescent complex as metalorganic monolayer.

Among transition metal oxides, nickel oxide is a chameleon material due to its multifunctional properties such as high dielectric constant, low resistivity, UV optical transparency, electrochromic and antiferromagnetic properties and p-type semiconducting behavior [32]. For these wide range of properties, NiO has been studied as material for organic light-emitting diodes (OLED) [33,34], smart windows [35,36], Schottky devices [37], chemical sensors [38], and tandem photocathodes for dye-sensitized solar cells (DSSC) [39,40].

Among luminescent molecules, the attention has been devoted to luminescent lanthanide complexes due to their exceptional photophysical properties such as high quantum yields, long excited-state lifetimes, large Stokes shifts and sharp emission profiles related to 4f-4f intraconfigurational electronic transitions. In particular, europium (III) is very interesting since it can act as an efficient downshifter [41] thus allowing the exploitation of the UV component of the solar spectrum.

In the present work, we apply for the first time a gas-phase route such as molecular layer deposition to create a monolayer of metalorganic Eu (III) molecules on the NiO surface through a self-limiting reaction with an excellent molecular-level control. Specifically, a full vapor phase approach is proposed based on the sequential steps of: i) metal organic chemical vapor deposition (MOCVD) of the inorganic NiO thin film; ii) activation of the NiO layer in order to form –OH terminal groups on the heated surface; (iii) MLD process to link the metalorganic monolayer of Eu(β-diketonate)$_3$•L on the activated surface in a covalent way. Three different Eu(III) complexes, Eu(tta)$_3$•phen (**EuC1**), Eu(hfa)$_3$•diglyme (**EuC2**) and Eu(hfa)$_3$•phen (**EuC3**) [42,43] (where Hhfa = 1,1,1,5,5,5-hexafluoro-2,4-pentanedione, Htta = 2-thenoyltrifluoroacetone, diglyme = bis(2-methoxyethyl) ether, and phen = 1,10-phenanthroline), have been evaluated based on their thermal properties, i.e. their suitability for the MLD process, and luminescence behavior. An accurate X-ray photoelectron (XPS) characterization confirmed the optimal parameter conditions of the activation step and of the covalent anchoring of the luminescent europium(III) adduct onto nanostructured transparent NiO films. Optical properties of the hybrid NiO/Eu(III) system are evaluated through spectroscopy measurement and show that an accurate control of the Eu coordination sphere may tune the luminescence properties of the monolayer.

2. Results and discussion

The novel synthetic procedure for the NiO/Eu(hfa)$_n$•phen (from now on **NiO@Eu** complex) hybrid system takes place inside a hot wall customized horizontal reactor and a scheme of the full vapor-phase process is shown in Fig. 1.

Highly uniform nanostructured NiO thin films, about 200 nm thick, have been deposited on 10 mm × 20 mm quartz substrates following a procedure reported in ref. [44] (Fig. 1a). After the MOCVD procedure for the inorganic NiO component, the second step regards the surface activation to yield -OH surface activated NiO films (**Act-NiO**). The NiO film is maintained at 300 °C inside the reactor at a pressure of 300 Torr for 1 h with a 600 ml/min H_2O/O_2 flux (Fig. 1b).

The activation step does not alter the structural and morphological features of the film. The crystalline phase analysis of the **Act-NiO** layer, through X-ray diffraction characterization (Fig. 2a), indicates an unaltered NiO cubic face centered structure (ICDD n° 47–1049), while the morphology derived from the field-emission scanning electron microscopy (FE-SEM) points to a uniform nanostructured NiO film with grains of about 70–80 nm (Fig. 2b). A scheme of the activated surface with respect to the as-deposited NiO layer is reported in Figs. 2d and 2c, respectively.

The evidence of NiO surface activation has been given by X-ray photoelectron spectroscopy (XPS) analysis. The XPS spectra of oxygen 1s, made on NiO surface, before (Fig. 2e) and after the activation through H_2O vapor (Fig. 2f), confirm the formation of –OH terminal groups due to the presence of Ni-OH and NiOOH signals. In particular, the O 1s band of the film before the activation consists of three components. The first component is observed at 529.3 eV and can be assigned to the O of the NiO lattice [45], while the components at 530.3 eV and 532.0 eV are attributable to the NiOOH and Ni-OH surface species, respectively. In the **Act-NiO,** the component at 529.3 eV due to the O of the NiO lattice is missing, while the components due to the hydroxylated species are prominent. The XPS region of Ni 2p reported in Fig. S1 (see Supporting Information) shows the typical Ni $2p_{3/2}$ and $2p_{1/2}$ spin-orbit doublet at 855.7 eV and 873.5 eV, respectively, with two shake-up satellites at ca. 6.5 eV and 7.3 eV higher than the Ni $2p_{3/2}$ and $2p_{1/2}$ main peaks. These values are slightly higher than the ones expected for bulk NiO [45,46], thus confirming the presence of hydroxylated Ni-OH and NiOOH surface species [22,47].

Different Eu(III) complexes have been evaluated for the formation of the Eu luminescent monolayer in order to select the one that better fits the MLD requirements, such as excellent volatility, high decomposition

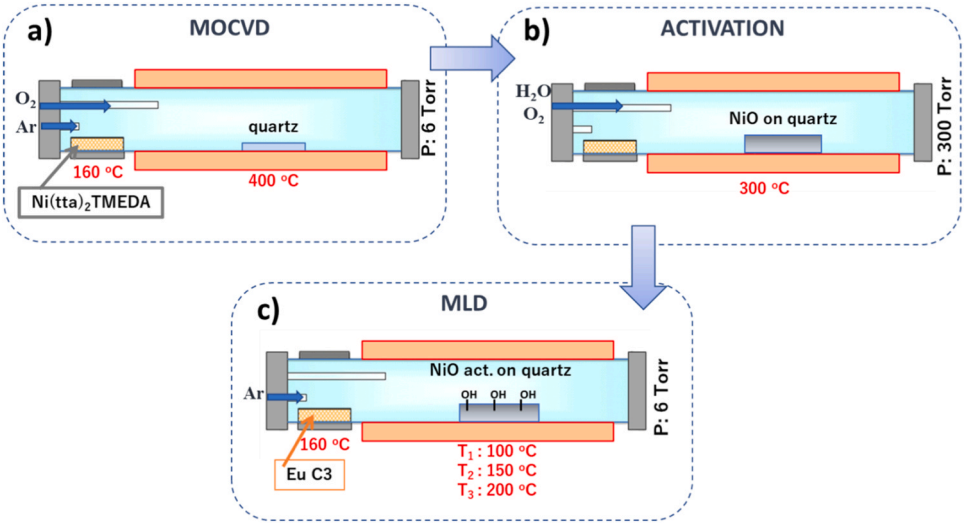

Fig. 1. Scheme of the full vapor phase approach to the preparation of the hybrid **NiO@Eu** system: a) MOCVD step to grow NiO films on quartz; b) activation of the NiO film through H_2O/O_2 flux at 300 °C and 300 Torr; c) MLD of the Eu complex on the **Act-NiO**.

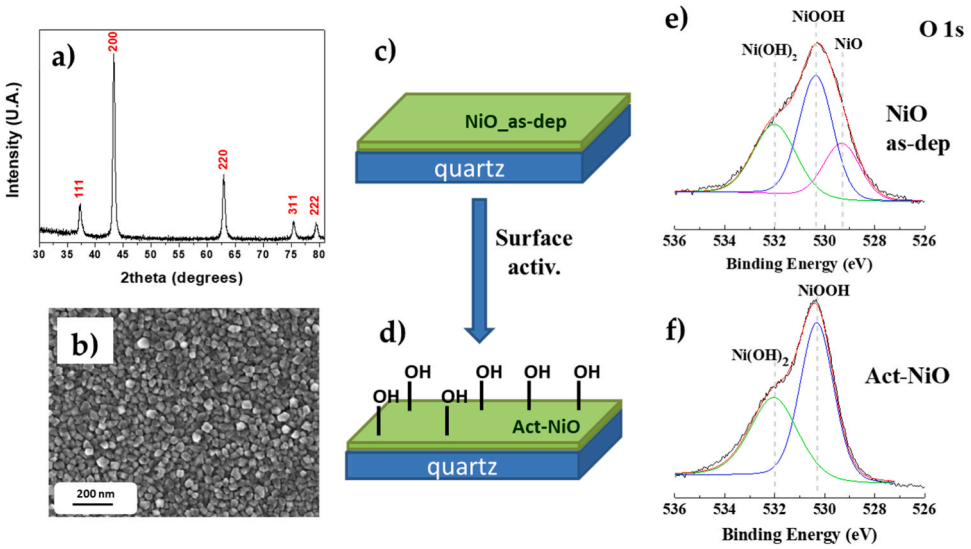

Fig. 2. a) XRD pattern and b) FE-SEM image of the Act-NiO film on quartz substrate. Schemes of c) NiO_as-dep film and d) NiO surface after the activation process through H_2O/O_2 flux at 300 °C and 300 Torr. XPS spectra of O 1s region on the surface of the e) NiO_as-dep and f) Act-NiO.

temperature and good reactivity. In particular, Eu(tta)$_3$•phen (**EuC1**), Eu(hfa)$_3$•diglyme (**EuC2**) and Eu(hfa)$_3$•phen (**EuC3**) have been considered and their structures are reported in Figs. 3a, 3b and 3c.

Thermal properties of the three Eu adducts have been tested through thermogravimetric measurements (Fig. 3d). The dynamic thermogravimetric (TGA) curve of **EuC1** shows a one-step decomposition in the 195–205 °C range, with a residue at 400 °C of about 40%, and thus **EuC1** possesses a behavior not suitable for vapor phase processes, but appropriate to produce solution route self-assembled monolayer [22]. On the other hand, both **EuC2** and **EuC3** show a single vaporization step, respectively at 180–190 °C and 245–255 °C, with very low residues in both cases of about 2%. Based on TGA data, both **EuC2** and **EuC3** present thermal behavior and volatility suited to MLD applications. The functional properties of the three complexes have been characterized through absorption spectra (Fig. S2 and ref. 43), where features attributed to the ligands are observed. Photoluminescent spectra of **EuC1**, **EuC2** and **EuC3** solutions in CH_2Cl_2 upon UV excitation are shown in Fig. S3 where emission bands due to 4f-4f intraconfigurational transitions of Eu(III) are clearly visible, due to efficient sensitizing from the organic ligands. Therefore, **EuC3** has been chosen as the best Eu(III) complex candidate for the anchoring on the NiO surface, due to its thermal behavior and the additional advantage of the presence of the 1, 10-phenanthroline, which acts as an antenna ligand thus enhancing the luminescent properties of the final hybrid system.

The third step procedure is the anchoring of the **EuC3** complex through molecular layer deposition (Fig. 1c). The activated NiO substrate is heated testing different temperatures, i.e. $T_1 = 100$ °C; $T_2 = 150$ °C and $T_3 = 200$ °C, and maintained at a pressure of 6 Torr for 1 h. The **EuC3** complex is vaporized at 160 °C and carried onto the **Act-NiO** surface through 150 ml/min argon flux, where the self-limiting chemisorption process occurs. Finally, the sonication treatment of the samples for 5 min in CH_2Cl_2, in which Eu(hfa)$_3$phen complex is highly soluble, guarantees that potential physisorbed **EuC3** molecules are removed, and only chemisorbed molecules remain anchored on the **Act-NiO** surface.

XPS analyses carried out on the NiO surface before and after the MLD and sonication steps have allowed a thorough understanding of the monolayer growth on the surface.

After the NiO surface activation, the MLD process to anchor the **EuC3** complex, and the sonication step, the XPS spectra of the **Act-NiO@EuC3** surface confirm that the **EuC3** complex is anchored on the surface. In particular, XPS spectrum of carbon, besides the signal at 285 eV, due to carbon atoms of the hydrocarbon backbone CH/C-C, ubiquitously observed due to adventitious species [48], shows the typical components of the hfa ligand at 292.5 eV and at 288.9 eV associated with the CF_3 groups and the C═O moiety, respectively (Fig. 4a). Another component at 286.5 eV can be also observed, likely due to the C-N groups of the phen ligand and to oxidized adventitious carbon species commonly observed on metal oxides surfaces. Furthermore, the presence of Eu 3d (Fig. 4b) in the hybrid system, after the sonication procedure, confirms that Eu containing molecules are still present on the surface and thus are covalently attached to the **Act-NiO** surface. The Eu spectrum shows the typical $3d_{5/2}$, $3d_{3/2}$ spin-orbit doublet at 1135.4 eV and 1165.5 eV respectively, indicating the presence of Eu (III) [22,49]. Note that low intensity components can be observed at about 1126.5 eV and 1156.5 eV, whose intensity increases by increasing the X-ray irradiation time during XPS analysis. These components are due to the X-ray induced reduction of the Eu(III) atoms of the anchored complex to Eu (II), in accordance with previously reported results [22,49].

Finally, the N 1s (Fig. 4c) signal, present in the **Act-NiO@EuC3**

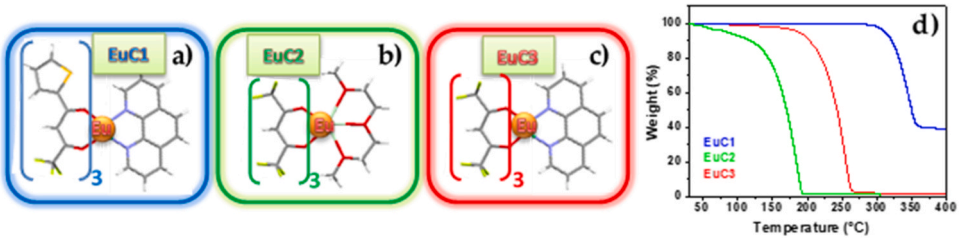

Fig. 3. Structures of a) Eu(tta)$_3$phen (**EuC1**), b) Eu(hfa)$_3$diglyme (**EuC2**) and c) Eu(hfa)$_3$phen (**EuC3**) complexes. d) Related thermogravimetric curves carried out at atmospheric pressure under 30 ml/min N_2.

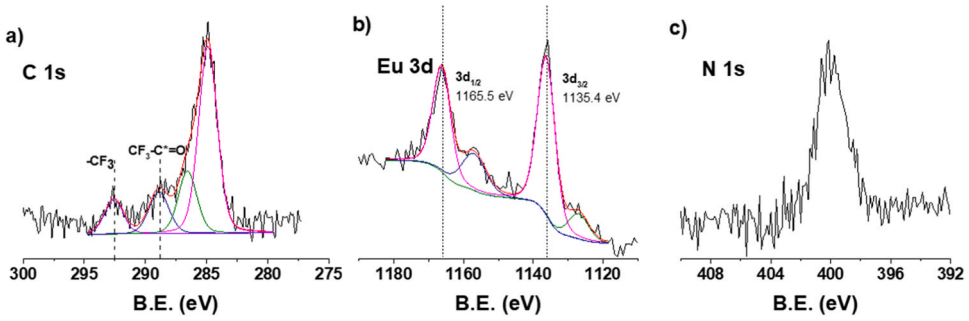

Fig. 4. XPS regions of C 1s (a), Eu 3d (b) and of N 1s (c) of the hybrid system NiO@Eu at 100 °C after the sonication treatment.

samples after sonication treatment, confirms that the antenna phen ligand is still present on the surface, thus indicating a really suited behavior of the **EuC3** complex for the MLD process. All these data univocally point to chemisorption of the **EuC3** on the **Act-NiO** surface.

Successively, the effect of different temperatures used in the MLD growth has been also studied to assess the most suited temperature for an efficient chemisorption process of the complex on the surface. To this aim the quantitative analysis on F 1s has been carried out at the different MLD temperatures, i.e. $T_1 = 100$ °C; $T_2 = 150$ °C $T_3 = 200$ °C, (Fig. 5a). Two different components are present: one at 689.0 eV is due to F of the CF_3 groups [50,51] and one at 685.4 eV is due to F of a fluoride component [52]. This effect is more evident at the highest tested temperatures (T_2 = 150 °C and T_3 = 200 °C), suggesting that some decomposition of the **EuC3** occurs, thus producing free fluorine. The fluoride component is likely due to some fluorine directly bonded to Eu, either as europium fluoride or as fluorine of a -CF_3 group acting as a bridge between two Eu ions (Fig. 5b). At the lowest temperature (T_1 = 100 °C) the -CF_3 component is predominant, indicating that at this temperature almost no decomposition occurs.

To deeply analyze the system, XPS quantitative analysis has been used to determine the coordination sphere of the **Eu** moieties in the monolayer. The comparison between the theoretical Eu:N:F ratio for species where Eu (III) has different coordination spheres and the experimental ratio in the samples is reported in Table 1. The **Act-Ni@Eu** sample obtained at the highest MLD T_3 temperature shows an Eu:N:F ratio of 1:0.5:7.5, thus indicating the presence of a very low amount of Eu moiety, Eu(hfa)•phen, and a large fluoride component (Fig. 5b). The observed experimental XPS Eu:N:F ratios of samples obtained at the lower T_1 and T_2 temperatures point to the presence of chemisorbed Eu $(hfa)_2$•phen and Eu(hfa)•phen frameworks (Fig. 5b), thus suggesting a ligand-exchange reaction between one or two β-diketonate ligands and the terminal –OH groups of the **Act-NiO** surface.

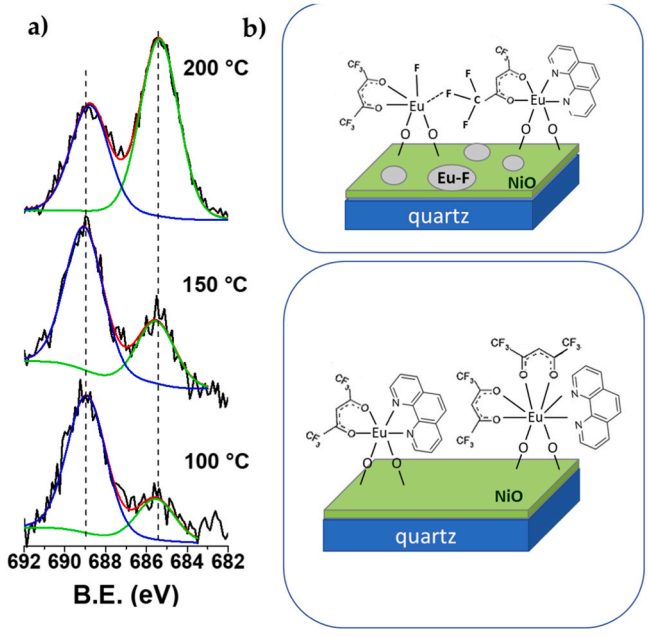

Fig. 5. a) XPS regions of F 1s at different temperatures: $T_1 = 100$ °C, $T_2 = 150$ °C, $T_3 = 200$ °C and b) schemes of the **Act-NiO@Eu** hybrid systems at related temperatures.

In addition, in order to evaluate the self-limited behavior of the monolayer formation, experiments have been carried out in the range 30–120 min. XPS has been used to estimate the amount of **EuC3** molecules on the surface through evaluation of the Eu/Ni (substrate) atomic ratio, considering the Eu 3d and Ni 2p signals at the various deposition time (Fig. S4). In Fig. 6 and Table 2, the measured Eu/Ni ratio is reported vs. deposition time, proving that chemisorption occurred with surface saturation already at 60 min. In fact, the ratio slightly increases from 30 min to 60 min, but it remains constant at 120 min.

In addition, in Table 2 the Eu:N:F ratio is reported for the three different cases. Thus, at 100 °C after 30 min and 60 min the F/Eu ratio is in both cases about 9/1 confirming that 1 or 2 hfa anion ligands are lost for the surface anchoring (see Table 1, Table 2 and Fig. 5b for the cartoon of the chemisorbed mojety). On the other hand, the N/Eu ratio of 2, expected from the theoretical chemical formula considering the coordination of phenanthroline, is observed up to 60 min. Unfortunately, at 120 min the Eu:N ratio is 1:1.3 indicating that time plays a similar role to temperature (at 200 °C the Eu:Ni ratio is 1:0.5), i.e. both determine the partial loss of the phenanthroline ligand. Thus, 100 °C and 60 min are the suited parameters to produce the Eu monolayer, maintaining its antenna ligand as confirmed by the luminescence measurements.

Present data indicate that this process is very promising for the formation of hybrid systems at temperature as low as 100 °C. Given the vapor phase nature and the very low thermal budget, this approach may be envisaged as an appealing, applicable route for the fabrication of a

Table1
Stoichiometries of the Eu moieties in the monolayer resulting by comparison of the experimental XPS Eu:N:F ratios in the monolayer vs. theoretical ratios in the starting adduct for different Eu coordinations.

Sample	MLD Temp (°C)	Eu:N:F ratio (XPS)	Nature of the monolayer
$Eu(hfa)_3$•phen	—	1:2:18 (theoretical)	
$Eu(hfa)_2$•phen	—	1:2:12 (theoretical)	
Eu(hfa)•phen	—	1:2:6 (theoretical)	
Act-NiO@Eu_200	200	1:0.5:7.5	Eu(hfa)•phen + Eu-F
Act-NiO@Eu_150	150	1:1.8:9.1	Eu(hfa)•phen $Eu(hfa)_2$•phen
Act-NiO@Eu_100	100	1:1.7:8.6	Eu(hfa)•phen $Eu(hfa)_2$•phen

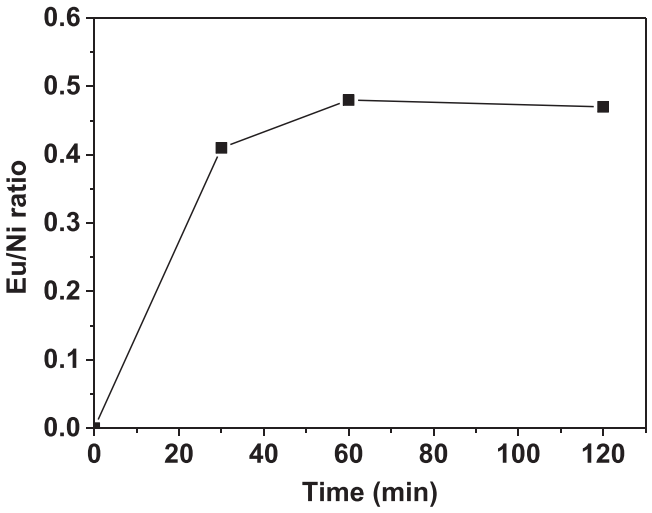

Fig. 6. Eu/Ni ratio calculated on the Eu 3d/Ni 2p areas for monolayers prepared at 30, 60 and 120 min.

Table 2
Eu/Ni ratios and stoichiometries of the Eu moieties in the monolayer deposited at 30, 60 and 120 min.

Dep. Time (min)	Eu/Ni	Eu:N:F
30	0.041	1: 2.0: 9.0
60	0.048	1: 1.7: 8.6
120	0.047	1: 1.3: 6.0

down-shifting monolayer in perovskite photovoltaic cells in a direct configuration, as well as for more conventional silicon PV cells.

The functional properties of the MLD grown Eu monolayers have been addressed through luminescence measurements in order to prove the energy conversion behavior as a proof-of-concept for their applications in photovoltaic cells. In addition, it is worth noting that trivalent europium is a very efficient luminescent probe widely used to study the symmetry of its local chemical environment, both in organic complexes [53] and in inorganic crystal hosts [54]. In fact, the emission spectra of the Eu(III) complex give important information about the local symmetry of the lanthanide. The luminescence properties have been investigated by measuring the excitation and emission spectra for the samples prepared at the three different temperatures.

In order to generate the Eu(III) emission in the optical range, we exploited the antenna effect of the phen ligand of the anchored complex by exciting into the phen lowest excited singlet state (S_1, see Fig. S5) with a 273 nm radiation.

As shown in Fig. S5, after population of the phen ligand, the Eu(III) complex undergoes an internal conversion (IC) and an intersystem crossing (ISC) processes that populate the lowest excited triplet state (T_1) at about 22000 cm^{-1} [55]. Then the excitation is transferred (energy transfer, ET) to the energy levels of the Eu(III), in particular to the $^5D_2$ excited state energy level, due to overlapping energies. After non-radiative relaxation to the $^5D_0$ excited energy level, several radiative processes from the $^5D_0$ level to the lower lying levels ^7F_J (J=0–6) take place, generating emissions in the visible range [56].

The excitation spectra, shown in Fig. 7a, were collected by monitoring the europium emission around 615 nm, corresponding to the $^5D_0 \rightarrow {}^7F_2$ transition, which is the most intense emission band observed for all the samples. The excitation spectra clearly show a strong band with a maximum at 273 nm, independently from the temperature of the MLD step. From a comparison with the absorption spectrum of 1,10-phenanthroline, shown in Fig. S6 the excitation band is a clear signature of the phen ligand that is acting as an antenna for Eu(III), confirming that the organic antenna is directly bonded to Eu(III) in all the three samples.

The different profiles of the excitation spectra of the three samples can be associated with the different amounts of phen ligand present in the Eu species chemisorbed on the NiO layer. In particular, the **Act-Ni@Eu** samples prepared at 100 °C and 150 °C show an excitation spectrum in agreement with the features observed in the absorption spectrum of 1,10-phenantroline (Fig. S6), with a clear and sharp peak at about 270 nm. On the other hand, the **Act-Ni@Eu** sample prepared at 200 °C shows instead only a broad band probably due to the presence of a lower amount of phen ligand with respect to the sample prepared at lower temperatures, as confirmed by the XPS quantitative measurements.

The emission bands in the visible range for samples obtained at different MLD deposition temperatures are shown in Fig. 7(b). These features are typical of Eu(III) ion emission, as indicated in the energy level scheme presented in Fig. S5. In particular, the spectra are dominated by a strong band centered around 615 nm, due to the $^5D_0 \rightarrow {}^7F_2$ transition. This is a so-called hypersensitive transition (ΔJ=2), whose intensity is strongly dependent on the local symmetry of the lanthanide [57].

In particular, a low symmetry environment corresponds to an enhanced intensity of the $^5D_0 \rightarrow {}^7F_2$ hypersensitive transition. Moreover, two emissions centered at 580 nm and 590 nm are observed in the emission spectra, due to $^5D_0 \rightarrow {}^7F_0$ and $^5D_0 \rightarrow {}^7F_1$ electronic transitions, respectively, although their intensities are lower than that of the band at 615 nm.

An important parameter that can be calculated through the emission spectra is the so-called asymmetry ratio R, defined as:

$$R = I\left(\frac{^5D_0 \rightarrow {}^7F_2}{I(^5D_0 \rightarrow {}^7F_1)}\right)$$

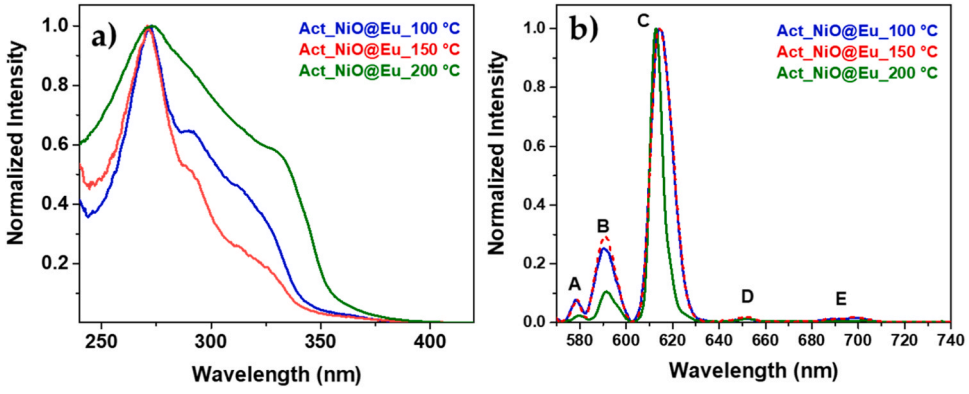

Fig. 7. Excitation a) and emission b) spectra of the Act-NiO@EuC3 samples: blue line, T_1 = 100 °C; red line, T_2 = 150 °C; green line, T_3 = 200 °C. Band assignment: A at ~ 579 nm $^5D_0 \rightarrow {}^7F_0$; B at ~ 591 nm $^5D_0 \rightarrow {}^7F_1$; C at ~ 614 nm $^5D_0 \rightarrow {}^7F_2$; D at ~ 651 nm $^5D_0 \rightarrow {}^7F_3$; E at ~ 700 nm $^5D_0 \rightarrow {}^7F_4$.

where the I values represent the integrated intensities of the bands centered at 615 nm and 590 nm, corresponding to the $^5D_0 \rightarrow ^7F_2$ and $^5D_0 \rightarrow ^7F_1$ electronic transitions, respectively [58–61].

From the emission spectra shown in Fig. 7b, the R values have been calculated to be 8.24, 3.92 and 4.26 for the **Act-Ni@Eu** samples prepared at 200 °C, 150 °C and 100 °C, respectively. In all cases it is evident that the Eu(III) is accommodated in sites with low symmetry. Comparing the asymmetry ratio values, the R value for the **Act-Ni@Eu** sample prepared at 200 °C indicate that the Eu(III) ions are located in less symmetric environment with respect to samples prepared at 100 °C and 150 °C. In this context, it is worth mentioning that the Eu^{3+} ions in crystalline EuF_3, accommodated in a quite symmetric environment as indicated by the emission spectra reported by Flores-Acosta et al. [62], present an asymmetry ratio well below 1. Since in the case under investigation the R values are much higher than 1, it can be deduced that the eventual contributions to the emission bands due to crystalline EuF_3 are practically negligible. On the other hand, since a fluoride component is found in the XPS data, we cannot exclude the presence of amorphous EuF_3 [63], for which the local environment of the europium is presumably much more distorted and therefore of lower symmetry. Alternatively, the presence of fluorine of -CF_3 groups of nearby molecules bridged to the Eu(III) of the monolayer could be responsible for the highly asymmetric environment of europium. This finding is compatible with the raise of the R value on passing from a preparation temperature of 100–200 °C.

Thus, the generation of available fluorine may arise from the decomposition of the hfa ligand, facilitated by the higher preparation temperature.

3. Conclusions

In the present scientific scenario, the development of a full vapor phase approach for the synthesis of hybrid materials through a fine tuning of their functional properties is of paramount importance. The reported study is, to our knowledge, unique, since no reports are known on the application of MLD to the growth of a metalorganic monolayer on oxide substrates and it represents a milestone in the field of the synthesis of downshifting and downconversion systems for potential applications in photovoltaics for several reasons explicated in the following. First of all, a full vapor phase straightforward approach has been applied for the synthesis of the hybrid metalorganic/inorganic system through sequential steps of MOCVD and MLD: (i) MOCVD of the inorganic NiO thin films; (ii) activation of the surface of transparent NiO as-deposited layer using H_2O vapor; (iii) MLD at different temperatures to link the Eu $(hfa)_3$phenanthroline in a covalent way on the activated surface. This Eu adduct has the advantage of both high thermal stability and excellent luminescence properties, which are boosted by the presence of 1,10-phenanthroline antenna ligand, useful to enhance the downshifting properties of the luminescent center. Notably, the MLD vapor phase route can be scaled on large area substrates and easily implemented at industrial level also considering the very low thermal budget needed for an efficient chemisorption process.

The effects of the activation process and the temperature for the MLD route have been deeply evaluated through XPS measurements, in order to define the best conditions for the chemisorption of the Eu system with the phen still coordinated to the Eu ion.

Besides, spectroscopy emission measurements in the visible range for the hybrid NiO/Eu(III) system has allowed to correlate the Eu(III) coordination sphere and the luminescence properties of the hybrid system and confirm the energy conversion phenomena of the monolayer.

In summary, the presently reported approach represents a facile, viable, time-saving, easily synthetic method, scalable at industrial level, to produce hybrid inorganic/metalorganic systems, which, given the great variety of inorganic and metalorganic species, may find applications in a huge number of fields. In the specific case of the **Act-NiO@Eu** complex, this system is of potential great interest for applications in tandem PV cells, since the NiO inorganic component is commonly applied as photocathode, while the Eu complex may further implement the use of the high energy side of the solar spectrum due to its downshifting properties.

Experimental details

Synthetic processes. The Eu complexes have been synthetized through a one-step reaction from the Eu(III) acetate hydrate, Hhfa, Htta, diglyme, phen following a procedure reported in ref. 42,43. NiO films have been grown in a reduced-pressure, horizontal, hot-wall reactor through an MOCVD process at 400 °C on transparent quartz substrate, starting from $Ni(tta)_2$tmeda [64], maintained at 160 °C in a resistively heated alumina boat. Specific details of the deposition process are reported in ref. [44a]. For the activation process the NiO films were maintained at 300 °C inside the reactor at the pressure of 300 Torr for 1 h under a O_2 flow saturated with H_2O at 600 ml/min. The sequential MLD procedure took place in the reactor where the activated NiO substrate was heated at $T_1 = 100$ °C; $T_2 = 150$ °C and $T_3 = 200$ °C and maintained at the pressure of 6 Torr for 1 h. The $Eu(hfa)_3$•phen complexes was vaporized at 160 °C and carried on the NiO surface through 150 ml/min argon flow, where the ligand-exchange reaction between ligands and surface –OH groups takes place. The chemisorption is guaranteed by an oversaturation of the Eu complex vapors inside the reactor. A sonication treatment of 5 min in CH_2Cl_2 on the final hybrid materials was conducted to ensure that the physisorbed Eu complex was removed and only chemisorbed complexes remained anchored to the NiO surface.

Characterization. Thermogravimetric analyses (TGA) of the complexes were performed using a Mettler Toledo TGA with STARe software under a prepurified nitrogen flow of 30 sccm, with a 5 °C/min heating rate at atmospheric pressure. The UV-Vis spectra of the europium adducts 1×10^{-4} M solutions in CH_2Cl_2 were collected using a JASCO V-650 UV–vis spectrophotometer. Photoluminescence spectra of the europium adducts 1×10^{-4} M solutions were collected with an excitation wavelength of 348 nm at room temperature using a JASCO FP-8300 spectrofluorimeter. X-Ray diffraction pattern was performed using a Smartlab Rigaku diffractometer in grazing incident mode (0.5°) operating at 45 kV and 200 mA equipped with a rotating anode of Cu K_α radiation. FE-SEM images were acquired using a field emission scanning electron microscope ZEISS SUPRA 55 VP. XPS spectra were recorded with a PHI 5600 multi-technique ESCA-Auger spectrometer with a standard Al-Kα X-ray source. Analyses were carried out with a photoelectron angle of 45° (relative to the sample surface) with an acceptance angle of ± 7°. The XPS binding energy (B.E.) scale was calibrated by centering the C 1s peak due to hydrocarbon moieties and adventitious carbon at 285.0 eV. The elemental compositions of the samples were evaluated by estimating the integrated area of each component corrected for the corresponding Wagner sensitivity factor [65]. Emission and excitation spectra of the monolayers were measured using a Jasco FP-8200 spectrofluorimeter, with a spectral bandwidth of 5 nm. For emission spectra, a low pass optical filter with cutoff at 550 nm was used.

CRediT authorship contribution statement

Anna L. Pellegrino: Conceptualization, Methodology, Writing – original draft. **Cristina Tudisco:** Visualization, Investigation. **Francesca Lo Presti:** Investigation. **Emil Milan:** Visualization, Investigation. **Adolfo Speghini:** Methodology, Validation. **Guglielmo G. Condorelli:** Data curation, Validation. **Graziella Malandrino:** Funding acquisition, Writing – review & editing.

Declaration of Competing Interest

The authors declare that they have no known competing financial

interests or personal relationships that could have appeared to influence the work reported in this paper.

Data availability

Data will be made available on request.

Acknowledgements

This work has been partially funded by European Union (NextGeneration EU), through the MUR-PNRR project SAMOTHRACE (ECS00000022). The authors thank the Bionanotech Research and Innovation Tower (BRIT) laboratory of Univer-sity of Catania (Grant no. PONa3_00136 financed by the Italian Ministry for Education, University and Research, MIUR) for the diffractometer facility. Francesco Mazzer (Vittorio Veneto, Treviso, Italy) is gratefully acknowledged for expert technical assistance. A. L. P. thanks the Ministero dell'Università e della Ricerca within the PON "Ricerca e Innovazione" 2014–2020 Azioni IV.4 program. Open access funding was provided by Università degli Studi di Catania within the CRUI-CARE Agreement.

Appendix A. Supporting information

Supplementary data associated with this article can be found in the online version at doi:10.1016/j.nanoen.2023.108804.

References

[1] W.L. Yang, J.D. Fabbri, T.M. Willey, J.R.I. Lee, J.E. Dahl, R.M.K. Carlson, P. R. Schreiner, A.A. Fokin, B.A. Tkachenko, N.A. Fokina, W. Meevasana, N. Mannella, K. Tanaka, X.J. Zhou, T. van Buuren, M.A. Kelly, Z. Hussain, N. A. Melosh, Z.-X. Shen, Monochromatic electron photoemission from diamondoid monolayers, Science 316 (2007) 1460–1462, https://doi.org/10.1126/science.1141811.

[2] M. Mannini, F. Pineider, C. Danieli, F. Totti, L. Sorace, P. Sainctavit, M.A. Arrio, E. Otero, L. Joly, J.C. Cezar, A. Cornia, R. Sessoli, Quantum tunnelling of the magnetization in a monolayer of oriented single-molecule magnets, Nature 468 (2010) 417–421, https://doi.org/10.1038/nature09478.

[3] N. Bahlawane, K. Kohse-Höinghaus, T. Weimann, P. Hinze, S. Röhe, M. Bäumer, Rational design of functional oxide thin films with embedded magnetic or plasmonic metallic nanoparticles, Angew. Chem. Int. Ed. 50 (2011) 9957–9960, https://doi.org/10.1002/anie.201102489.

[4] E. Biavardi, C. Tudisco, F. Maffei, A. Motta, C. Massera, G.G. Condorelli, E. Dalcanale, Exclusive recognition of sarcosine in water and urine by a cavitand-functionalized silicon surface, Proc. Natl. Acad. Sci. 109 (2012) 2263–2268, https://doi.org/10.1073/pnas.1112264109.

[5] S. Wang, Y. Kang, L. Wang, H. Zhang, Y. Wang, Y. Wang, Organic/inorganic hybrid sensors: A review, Sens. Actuators B 182 (2013) 467–481, https://doi.org/10.1016/j.snb.2013.03.042.

[6] S. Oh, N. Khan, S.-M. Jin, H. Tran, N. Yoon, C.E. Song, H.K. Lee, W.S. Shin, J.-C. Lee, S.-J. Moon, E. Lee, S.K. Lee, Alkyl side-chain dependent self-organization of small molecule and its application in high-performance organic and perovskite solar cells, Nano Energy 72 (2020), 104708, https://doi.org/10.1016/j.nanoen.2020.104708.

[7] S. Yaacoub, S. Calas-Etienne, J. Jabbour, K. Amro, R. Tauk, A. Khoury, A. Mehdic, P. Etienne, Design and controlled synthesis by dual polymerization of new organic–inorganic hybrid material for photonic devices, RSC Adv. 4 (2014) 17210–17217, https://doi.org/10.1039/C4RA01059K.

[8] F. Huang, H. Liu, X. Li, S. Wang, Highly efficient hole injection/transport layer-free OLEDs based on self-assembled monolayer modified ITO by solution-process, Nano Energy 78 (2020), 105399, https://doi.org/10.1016/j.nanoen.2020.105399.

[9] D. Hueber, M. Hoffmann, B. Louis, P. Pale, A. Blanc, Inorganic–organic heteropolyacid–gold(I) hybrids: structures and catalytic applications, Chem. Eur. J. 20 (2014) 3903–3907, https://doi.org/10.1002/chem.201304680.

[10] A.P. Wight, M.E. Davis, Design and preparation of organic−inorganic hybrid catalysts, Chem. Rev. 102 (2002) 3589–3614, https://doi.org/10.1021/cr010334m.

[11] W. Li, J. Shi, K.H.L. Zhang, J.L. MacManus-Driscoll, Defects in complex oxide thin films for electronics and energy applications: challenges and opportunities, Mater. Horiz. 7 (2020) 2832–2859, https://doi.org/10.1039/D0MH00899K.

[12] J. Meyer, S. Hamwi, M. Kröger, W. Kowalsky, T. Riedl, A. Kahn, Transition metal oxides for organic electronics: energetics, device physics and applications, Adv. Mater. 24 (2012) 5408–5427, https://doi.org/10.1002/adma.201201630.

[13] P. Poizot, S. Laruelle, S. Grugeon, L. Dupont, J.-M. Tarascon, Nano-sized transition-metal oxides as negative-electrode materials for lithium-ion batteries, Nature 407 (2000) 496–499, https://doi.org/10.1038/35035045.

[14] X. Qian, K. Fuku, Y. Kuwahara, T. Kamegawa, K. Mori, H. Yamashita, Design and functionalization of photocatalytic systems within mesoporous silica, ChemSusChem 7 (2014) 1528–1536, https://doi.org/10.1002/cssc.201400111.

[15] A. Abdolmalekia, S. Mallakpoura, S. Borandeh, Tailored functionalization of ZnO nanoparticle via reactive cyclodextrin and its bionanocomposite synthesis, Carbohydr. Polym. 103 (2014) 32–37, https://doi.org/10.1016/j.carbpol.2013.12.013.

[16] G. Pellegrino, G.G. Condorelli, V. Privitera, B. Cafra, S. Di Marco, A. Alberti, Dye-sensitizing of self-nanostructured Ti(:Zn)O_2/AZO transparent electrodes by self-assembly of 5,10,15,20-tetrakis(4-carboxyphenyl)porphyrin, J. Phys. Chem. C. 115 (2011) 7760–7767, https://doi.org/10.1021/jp110819n.

[17] B.H. Farnum, K.-R. Wee, T.J. Meyer, Self-assembled molecular p/n junctions for applications in dye-sensitized solar energy conversion, Nat. Chem. 8 (2016) 845–852, https://doi.org/10.1038/nchem.2536.

[18] C. Sanchez, F. Ribot, B. Lebeau, Molecular design of hybrid organic-inorganic nanocomposites synthesized via sol-gel chemistry, J. Mater. Chem. 9 (1999) 35–44, https://doi.org/10.1039/A805538F.

[19] J.Y. Wen, G.L. Wilkes, Organic/inorganic hybrid network materials by the sol−gel approach, Chem. Mater. 8 (1996) 1667–1681, https://doi.org/10.1021/cm9601143.

[20] M. Clemente Leon, B. Agricole, C. Mingotaud, C.J. Gomez Garcia, E. Coronado, P. Delhaes, Toward new organic/inorganic superlattices: Keggin polyoxometalates in Langmuir and Langmuir-Blodgett films, Langmuir 13 (1997) 2340–2347, https://doi.org/10.1021/la960576v.

[21] M. Clemente-Leon, C. Mingotaud, B. Agricole, C.J. Gomez Garcia, E. Coronado, P. Delhaes, Application of the Langmuir-Blodgett technique to polyoxometalates: towards new magnetic films, Angew. Chem. Int. Ed. 36 (1997) 1114, https://doi.org/10.1002/anie.199711141.

[22] E. Smecca, C. Tudisco, A.E. Giuffrida, M.R. Catalano, A. Speghini, G. Malandrino, G.G. Condorelli, Spatially confined functionalization of transparent NiO thin films with a luminescent (1,10–Phenanthroline) tris (2–thenoyltrifluoroacetonato) europium monolayer, Eur. J. Inorg. Chem. (7) (2015) 1261–1268, https://doi.org/10.1002/ejic.201402479.

[23] A. Gulino, F. Lupo, D.A. Cristaldi, S. Pappalardo, C. Capici, G. Gattuso, A. Notti, M. F. Parisi, A viable route for lithium ion detection, Eur. J. Inorg. Chem. 3 (2014) 442–449, https://doi.org/10.1002/ejic.201301213.

[24] J.G. Matisons, Silanes and siloxanes as coupling agents to glass: a perspective, Adv. Silicon Sci. 4 (2012) 281–298, https://doi.org/10.1007/978-94-007-3876-8_10.

[25] (a) L. Newton, T. Slater, N. Clark, A. Vijayaraghavan, Self-assembled monolayers (SAMs) on metallic surfaces (gold and graphene) for electronic applications, J. Mater. Chem. C. 1 (2013) 376–393, https://doi.org/10.1039/C2TC00146B;
(b) C. Vericat, M.E. Vela, G. Benitez, P. Carro, R.C. Salvarezza, Self-assembled monolayers of thiols and dithiols on gold: new challenges for a well-known system, Chem. Soc. Rev. 39 (2010) 1805–1834, https://doi.org/10.1039/B907301A.

[26] (a) M. Klaumünzer, A. Kahnt, A. Burger, M. Mackovic, C. Münzel, R. Srikantharajah, E. Spiecker, A. Hirsch, W. Peukert, D.M. Guldi, Surface functionalization and electronic interactions of ZnO nanorods with a porphyrin derivative, ACS Appl. Mater. Interfaces 6 (2014) 6724–6730, https://doi.org/10.1021/am5004552;
(b) C. Tudisco, A.L. Pellegrino, G. Malandrino, G.G. Condorelli, Surface anchoring of bi-functional organic linkers on piezoelectric BiFeO3 films and particles: Comparison between carboxylic and phosphonic tethering groups, Surf. Coat. Technol. 343 (2018) 75–82, https://doi.org/10.1016/j.surfcoat.2017.11.014.

[27] (a) G. Guerrero, J.G. Alauzun, M. Granier, D. Laurencin, P.H. Mutin, Phosphonate coupling molecules for the control of surface/interface properties and the synthesis of nanomaterials, Dalton Trans. 42 (2013) 12569–12585, https://doi.org/10.1039/C3DT51193F;
(b) D.K. Bhowmick, A.J. Urban, M. Bartsch, B. Braunschweig, H. Zacharias, Near-UV-induced rapid formation of compact self-assembled organophosphonate monolayers on H-terminated Si (111) Surfaces, J. Phys. Chem. C. 126 (2022) 19978–19986, https://doi.org/10.1021/acs.jpcc.2c03335.

[28] D.Han Kim, M.D. Losego, Q. Peng, G.N. Parsons, Atomic layer deposition for sensitized solar cells: recent progress and prospects, Adv. Mater. Interfaces 3 (2016) 1600354, https://doi.org/10.1002/admi.201600354.

[29] (a) S.M. George, Atomic layer deposition: an overview, Chem. Rev. 110 (2009) 111–131, https://doi.org/10.1021/cr900056b;
(b) B.H. Lee, B. Yoon, A.I. Abdulagatov, R.A. Hall, S.M. George, Growth and properties of hybrid organic-inorganic metalcone films using molecular layer deposition techniques, Adv. Funct. Mater. 23 (2013) 532–546, https://doi.org/10.1002/adfm.201200370;
(c) H. Zhou, S.F. Bent, Fabrication of organic interfacial layers by molecular layer deposition: Present status and future opportunities, 040801-1, J. Vac. Sci. Technol. A 31 (2013), https://doi.org/10.1116/1.4804609.

[30] (a) M. Madadi, J. Heiska, J. Multia, M. Karppinen, Atomic and molecular layer deposition of alkali metal based thin films, ACS Appl. Mater. Interfaces 13 (2021) 56793–56811, https://doi.org/10.1021/acsami.1c17519;
(b) P. Sundberg, M. Karppinen, Organic and inorganic-organic thin film structures by molecular layer deposition: a review, Beil. J. Nanotechnol. 5 (2014) 1104–1136, https://doi.org/10.3762/bjnano.5.123.

[31] (a) J. Multia, M. Karppinen, Atomic/molecular layer deposition for designer's functional metal–organic materials, Adv. Mater. Interfaces 9 (2022) 2200210, https://doi.org/10.1002/admi.202200210;
(a) P. Kaur, A. Muriqi, J.-L. Wree, R. Ghiyasi, M. Safdar, M. Nolan, M. Karppinen, A. Devi, Atomic/molecular layer deposition of cerium(III) hybrid thin films using rigid organic precursors, Dalton Trans. 51 (2022) 5603–2205611, https://doi.org/10.1039/D2DT00353H.

[32] I. Sugiyama, N. Shibata, Z. Wang, S. Kobayashi, T. Yamamoto, Y. Ikuhara, Ferromagnetic dislocations in antiferromagnetic NiO, Nat. Nanotechnol. 8 (2013) 266–270, https://doi.org/10.1038/nnano.2013.45.

[33] J.M. Caruge, J.E. Halpert, V. Bulovic, M.G. Bawendi, NiO as an inorganic hole-transporting layer in quantum-dot light-emitting devices, Nano Lett. 6 (2006) 2991–2994, https://doi.org/10.1021/nl0623208.

[34] J. Huang, G. Natu, Z.Q. Ji, P. Hasin, Y.Y. Lu, p-type dye-sensitized NiO solar cells: a study by electrochemical impedance spectroscopy, J. Phys. Chem. C. 115 (2011) 25109–25114, https://doi.org/10.1021/jp205306g.

[35] Y. Sato, S. Tamura, K. Murai, Electrochromic properties of nickel oxide films prepared by the oxidation of nickel-carbon composite films, Jpn. J. Appl. Phys. 35 (Pt. 2) (1996) 6275–6279, https://doi.org/10.7567/JJAP.35.6275.

[36] F. Decker, S. Passerini, R. Pileggi, B. Scrosati, The electrochromic process in non-stoichiometric nickel oxide thin film electrodes, Electrochim. Acta 37 (1992) 1033–1038, https://doi.org/10.1016/0013-4686(92)85220-F.

[37] R. Lo Nigro, S. Battiato, G. Greco, P. Fiorenza, F. Roccaforte, G. Malandrino, Metal organic chemical vapor deposition of nickel oxide thin films for wide band gap device technology, Thin Solid Films 563 (2014) 50–55, https://doi.org/10.1016/j.tsf.2014.04.012.

[38] J. Fu, C. Zhao, J. Zhang, Y. Peng, E. Xie, Enhanced gas sensing performance of electrospun Pt-functionalized NiO nanotubes with chemical and electronic sensitization, ACS Appl. Mater. Interfaces 5 (2013) 7410–7416, https://doi.org/10.1021/am4017347.

[39] A. Nattestad, A.J. Mozer, M.K.R. Fischer, Y.-B. Cheng, A. Mishra, P. Bäuerle, U. Bach, Highly efficient photocathodes for dye-sensitized tandem solar cells, Nat. Mater. 9 (2010) 31–35, https://doi.org/10.1038/nmat2588.

[40] E.A. Gibson, A.L. Smeigh, L. Le Pleux, J. Fortage, G. Boschloo, E. Blart, Y. Pellegrin, F. Odobel, A. Hagfeldt, L. Hammarström, A p-type NiO-based dye-sensitized solar cell with an open-circuit voltage of 0.35 V, Angew. Chem. Int. Ed. 48 (2009) 4466–4469, https://doi.org/10.1002/ange.200900423.

[41] (a) D. Yang, H. Liang, Y. Liu, M. Hou, L. Kan, Y. Yang, Z. Zang, A large-area luminescent downshifting layer containing an Eu^{3+} complex for crystalline silicon solar cells, Dalton Trans. 49 (2020) 4725–4731, https://doi.org/10.1039/C9DT04858H;
(b) A. Gavriluta, T. Fix, A. Nonat, A. Slaoui, J.-F. Guillemolesad, J. Loïc, Charbonnière, Tuning the chemical properties of europium complexes as downshifting agents for copper indium gallium selenide solar cells, J. Mater. Chem. A 5 (2017) 14031–14040, https://doi.org/10.1039/C7TA02892J.

[42] G. Malandrino, M. Bettinelli, A. Speghini, I.L. Fragala, Europium "Second Generation" precursors for metal-organic chemical vapor deposition: characterization and optical spectroscopy, Eur. J. Inorg. Chem. 4 (2001) 1039–1044, https://doi.org/10.1002/1099-0682(200104)2001:4<1039::AID-EJIC1039>3.0.CO;2-2.

[43] F. Fagnani, A. Colombo, G. Malandrino, C. Dragonetti, A.L. Pellegrino, Luminescent 1,10-phenanthroline β-diketonate europium complexes with large second-order nonlinear optical properties, Molecules 27 (2022) 6990, https://doi.org/10.3390/molecules27206990.

[44] (a) S. Battiato, M.M. Giangregorio, M.R. Catalano, R. Lo Nigro, M. Losurdo, G. Malandrino, Morphology-controlled synthesis of NiO films: the role of the precursor and the effect of the substrate nature on the films' structural/optical properties, RSC Adv. 6 (2016) 30813–30823, https://doi.org/10.1039/C6RA05510A;
(b) R. Lo Nigro, G. Fisichella, S. Battiato, G. Greco, P. Fiorenza, F. Roccaforte, G. Malandrino, An insight into the epitaxial nanostructures of NiO and CeO2 thin film dielectrics for AlGaN/GaN heterostructures, Mater. Chem. Phys. 162 (2015) 461–468, https://doi.org/10.1016/j.matchemphys.2015.06.015.

[45] S. Uhlenbrockt, C. Scharfschwerdtt, M. Neumannt, G. Illing, H.-J. Freund, The influence of defects on the Ni 2p and O 1s XPS of NiO, J. Phys.: Condens. Matter 4 (1992) 7973–7978, https://doi.org/10.1088/0953-8984/4/40/009.

[46] M. Chigane, M. Ishikawa, XRD and XPS characterization of electrochromic nickel oxide thin films prepared by electrolysis–chemical deposition, J. Chem. Soc. Faraday Trans. 94 (1998) 3665–3670, https://doi.org/10.1039/A806459H.

[47] M.A. Peck, M.A. Langell, Comparison of nanoscaled and bulk NiO structural and environmental characteristics by XRD, XAFS, and XPS, Chem. Mater. 24 (2012) 4483–4490, https://doi.org/10.1021/cm300739y.

[48] (a) I.L. Swift, Adventitious carbon—the panacea for energy referencing? Surf. Interface Anal. 4 (1982) 47–51, https://doi.org/10.1002/sia.740040204;
(b) D. Briggs, G. Beamson, Primary and secondary oxygen-induced C1s binding energy shifts in x-ray photoelectron spectroscopy of polymers, Anal. Chem. 64 (1992) 1729–1736, https://doi.org/10.1021/ac00039a018.

[49] K. Misztal, C. Tudisco, A. Sartori, J.M. Malicka, R. Castelli, G.G. Condorelli, E. Dalcanale, Hierarchical self-assembly of luminescent euiii complexes on silicon, Eur. J. Inorg. Chem. (2014) 2687–2694, https://doi.org/10.1002/ejic.201402117.

[50] G. Nansé, E. Papirer, P. Fioux, F. Moguet, A. Tressaud, Fluorination of carbon blacks: An X-ray photoelectron spectroscopy study: I. A literature review of XPS studies of fluorinated carbons. XPS investigation of some reference compounds, Carbon 35 (1997) 175–194, https://doi.org/10.1016/S0008-6223(96)00095-4.

[51] X.L. Zhu, S.B. Liu, B.Y. Man, C.Q. Xie, D.P. Chen, D.Q. Wang, T.C. Ye, M. Liu, Analysis by using X-ray photoelectron spectroscopy for polymethyl methacrylate and polytetrafluoroethylene etched by KrF excimer laser, Appl. Surf. Sci. 253 (2007) 3122–3126, https://doi.org/10.1016/j.apsusc.2006.07.002.

[52] J.F. Moulder, W.F. Stickle, P.E. Sobol, K.D. Bomben, Handbook of X-ray photoelectron spectroscopy, in: J. Charstain (Ed.), Perkin- Elmer Corporation, Physical Electronic Division, Eden Praire, MN, 1992.

[53] (a) P.L. Forster, D.F. Parra, A.B. Lugao, J. Kai, H.F. Brito, Highly luminescent polycaprolactone films doped with diaquatris (thenoyltrifluoroacetonate) europium (III) complex, J. Lumin. 167 (2015) 85–90, https://doi.org/10.1016/j.jlumin.2015.05.041;
(b) D. Singh, S. Bhagwan, A. Dalal, K. Nehra, R.K. Saini, K. Singh, S. Kumar, I. Singh, Synthesis and investigation of enhanced luminescence of Ln(III)-complexes containing fluorinated β-diketone and oxygen donor ancillary ligands for efficient advanced displays, J. Lumin. 223 (2020), 117255, https://doi.org/10.1016/j.jlumin.2020.117255.

[54] (a) Y. Kitagawa, J. Ueda, M.G. Brik, S. Tanabe, Intense hypersensitive luminescence of Eu^{3+}-doped $YSiO_2N$ oxynitride with near-UV excitation, Opt. Mater. 83 (2018) 111–117, https://doi.org/10.1016/j.optmat.2018.05.039;
(b) I.L.V. Rosa, L.H. Oliveira, E. Longo, J.A. Varela, Synthesis and photoluminescence behavior of the Eu^{3+} ions as a nanocoating over a silica Stöber matrix, J. Fluoresc. 21 (2011) 975–981, https://doi.org/10.1007/s10895-010-0671-8.

[55] J.S. Brinen, D.D. Rosebrook, R.C. Hirt, Phosphorence of o-phenanthroline, J. Phys. Chem. 67 (1963) 2651–2655, https://doi.org/10.1021/j100806a035.

[56] (a) A.K.R. Junker, L.R. Hill, A.L. Thompson, S. Faulkner, T.J. Sørensen, Shining light on the antenna chromophore in lanthanide based dyes, Dalton Trans. 47 (2018) 4794–4803, https://doi.org/10.1039/C7DT04788F;
(b) K. Nehra, A. Dalal, A. Hooda, S. Singh, D. Singh, Computational and spectroscopic evaluation of 1,10-phenanthroline based Eu(III) fluorinated β-Diketonate Complexes for displays, J. Lumin. 251 (2022), 119111, https://doi.org/10.1016/j.jlumin.2022.119111.

[57] D. Errulat, G. Gabidullin, M. Murugesu, E. Hemmer, Probing optical anisotropy and polymorph-dependent photoluminescence in $[Ln_2]$ complexes by hyperspectral imaging on single crystals, Chem. Eur. J. 24 (2018) 10146–10155, https://doi.org/10.1002/chem.201801224.

[58] C.K. Jørgensen, B.R. Judd, Hypersensitive pseudoquadrupole transitions in lanthanides, Mol. Phys. 8 (1964) 281–290, https://doi.org/10.1080/00268976400100321.

[59] A.F. Kirby, F.S. Richardson, Optical excitation and emission spectra of europium (3+) in microcrystalline samples of trigonal $Na_3[Eu(ODA)_3]$. $2NaClO_4{\cdot}6H_2O$, J. Phys. Chem. 87 (1983) 2557–2563.

[60] E. Hemmer, K. Soga, T. Konishi, T. Watanabe, T. Taniguchi, S. Mathur, Influence of the host phase on the vibrational spectra of europium-doped zirconia prepared by hydrothermal processing, J. Am. Ceram. Soc. 93 (2010) 3873–3879, https://doi.org/10.1111/j.1551-2916.2010.03981.x.

[61] K. Binnemans, Interpretation of europium(III) spectra, Coord. Chem. Rev. 295 (2015) 1–45, https://doi.org/10.1016/j.ccr.2015.02.015.

[62] M. Flores-Acosta, R. Pérez-Salas, R. Aceves, M. Sotelo-Lerma, R. Ramírez-Bon, Structural and photoluminescent properties of EuF3 nanoparticles in zeolite, Solid State Commun. 136 (2005) 567–571, https://doi.org/10.1016/j.ssc.2005.09.034.

[63] W. Burian, J. Szade, T. O'Keevan, Z. Celiński, Photoemission study of Eu valency in EuF_3 ultrathin buried layers and single crystals, Phys. Stat. Sol. B 241 (2004) R15–R18, https://doi.org/10.1002/pssb.200409032.

[64] G. Malandrino, L.M.S. Perdicaro, G. Condorelli, I.L. Fragala, P. Rossi, P. Dapporto, Synthesis, characterization and application of $Ni(tta)_2{\cdot}tmeda$ to MOCVD of nickel oxide thin films, Dalton Trans. (8) (2006) 1101–1106, https://doi.org/10.1039/B511317B.

[65] C.D. Wagner, L.E. Davis, M.V. Zeller, J.A. Taylor, R.H. Raymond, L.H. Galeet, Empirical atomic sensitivity factors for quantitative analysis by electron spectroscopy for chemical analysis, Surf. Int. Anal. 3 (1981) 211–225, https://doi.org/10.1002/sia.740030506.